Mechanochemical Active Feedback Generates Convergence Extension in Epithelial Tissue

Aondoyima Ioratim-Uba,[1] Tanniemola B. Liverpool,[1] and Silke Henkes[1,2]
[1]School of Mathematics, University of Bristol, Bristol BS8 1UG, United Kingdom
[2]Lorentz Institute for Theoretical Physics, Leiden University, Leiden 2333 CA, The Netherlands

(Received 13 April 2023; accepted 7 November 2023; published 7 December 2023)

Convergence extension, the simultaneous elongation of tissue along one axis while narrowing along a perpendicular axis, occurs during embryonic development. A fundamental process that contributes to shaping the organism, it happens in many different species and tissue types. Here, we present a minimal continuum model, that can be directly linked to the controlling microscopic biochemistry, which shows spontaneous convergence extension. It is comprised of a 2D viscoelastic active material with a mechanochemical active feedback mechanism coupled to a substrate via friction. Robust convergent extension behavior emerges beyond a critical value of the activity parameter and is controlled by the boundary conditions and the coupling to the substrate. Oscillations and spatial patterns emerge in this model when internal dissipation dominates over friction, as well as in the active elastic limit.

DOI: 10.1103/PhysRevLett.131.238301

Convergent extension (CE) is a morphogenetic process that occurs during development. It is conserved across many different species, types of tissues, and stages of development [1–4]. During convergent extension, a region of sheetlike (epithelial) tissue elongates in one direction (the long axis) and contracts perpendicular to it. Convergent extension plays a key role in a variety of developmental processes, such as primitive streak formation in chick embryos [5,6] and drosophila germ band extension [7,8] which are important parts of gastrulation. This is the topological inversion process shared by nearly all multicellular animals and some plants [9] that leads to cells taking up their correct positions within the embryo.

CE in epithelia is driven by cell intercalations [2,10], i.e., local cell rearrangements akin to the well-known topological T1 transitions of two-dimensional (passive) foams [11,12]. T1s in passive systems relax stresses generated by external driving and underlie the rheology of foams, which are typically yield stress materials [13]. However, in epithelia, active T1 transitions [7,8,14] can generate stresses locally in the absence of external driving, even developing local stresses that oppose external boundary forces. These are only possible due to motor-driven contractile stress generation, i.e., the epithelial tissue is *active*. It is natural to ask how such events coordinate with each other to give coherent macroscopic deformations in response to applied tension.

Until recently, the accepted answer has been preexisting morphogenetic gene expression patterns that bias local mechanical properties [10,15–17]. However, the actomyosin fibers of the cytoskeleton themselves experience mechanical feedback [18–20], and in, e.g., the chick embryo there is no evidence for prepatterning [5]. Therefore, recent work has begun including active feedback into models of coupled junctions [21–25]. The response in tissues without T1s has also been investigated [26–28].

Hence, it is essential to study the active tissue mechanical response with feedback built in. Active models of cell sheets (without feedback) have a long tradition, from active gel theory [29,30] to active nematics [31–33] and hexatics [34]. They have focused on active instabilities and topological defect motion, including *in vitro* experiments [35], rather than the functional response of the tissue. More recently, spatial patterns [6,36] or anisotropic and signaling feedback [37,38], recapitulating embryo observations, have been imposed and the resulting flow quantified. Generic models with feedback have also been recently proposed [39–41]. However, so far a broader understanding of the emergent active relation between applied stress and strain rate, i.e., the tissue rheology, in the presence of feedback, is missing.

Here, we present and analyze a continuum description of an epithelium with active feedback where motor-driven contractile stress builds up in response to applied tension as in, e.g., a catch bond [42,43]. It is the continuum version of a microscopic cell junction model [44] driven by stresses generated by myosin-II motors acting on cytoskeletal F-actin (actomyosin) that generate active T1s and CE flow in a tissue patch. We formulate the model in terms of the anisotropic distribution of actomyosin within cells, passive viscoelastic stress, and the velocity via momentum balance

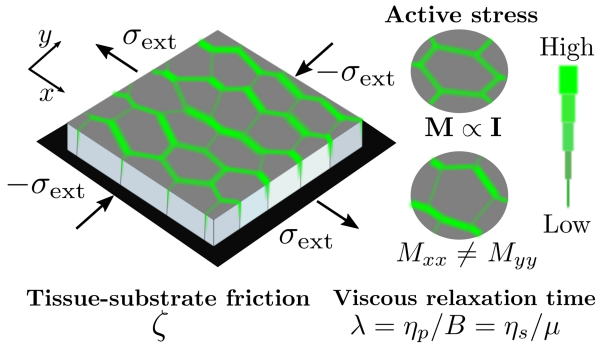

FIG. 1. Schematic of a 2D sheet of tissue with actomyosin localized along the junctions of the apical surface (shades of green). The myosin tensor $\boldsymbol{M}$ encodes both the concentration and the anisotropic distribution of actomyosin in cells, and gives rise to active stress $\beta(\boldsymbol{M} - m_0\boldsymbol{I})$. The tissue is viscoelastic with a viscous relaxation time τ_v.

with a substrate (see Fig. 1). We find that above a critical activity CE states appear, characterized by flow *against* externally applied stress which acts like a mechanical signal (Fig. 2). In this parameter regime, we also find contracting and expanding states that are isotropic and not nematic. We explain this using a steady-state approximation of the feedback dynamics, where high (low) boundary stresses select a high (low) actomyosin fixed point in the interior, which builds up a spatial gradient leading to flow. Separately, we find oscillating and patterned states in this model in the active elastic and low substrate friction limits.

Model.—We write down continuum equations for the epithelium as a 2D viscoelastic material that generates active stresses internally, and is coupled to a substrate via friction. Our fundamental quantity is the second rank

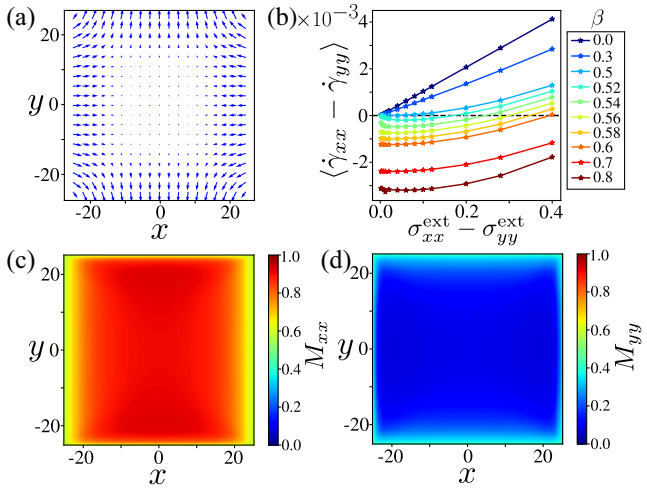

FIG. 2. (a) Steady state convergence extension velocity field at $\beta = 0.7$, $\sigma_s = 0.08$, $p = 0$, and $\tau_m = \tau_v = 20.0$. (b) Pure shear strain as a function of pure shear stress at the boundary for various values of activity. (c) xx component and (d) yy component of the actomyosin tensor for panel (a).

actomyosin tensor $\boldsymbol{M}(\mathbf{r}, t)$. It encodes the spatially anisotropic distribution of actomyosin which in embryonal tissues is localized at the apical surface along the junctions [6,36]. It can be defined using junction directions weighted by actomyosin concentration [36,44,45] (see Fig. 1). It is symmetric but not traceless, i.e., for cells with isotropic actomyosin distributions, $\boldsymbol{M} \propto \boldsymbol{I}$, the identity.

The other fields that characterize the material are local velocity $\mathbf{v}(\mathbf{r}, t)$ and local passive stress $\boldsymbol{\pi}(\mathbf{r}, t)$. The total stress $\boldsymbol{\sigma}(\mathbf{r}, t)$ is the sum of the passive stress and an active stress that generates the forces that remodel cell-cell junctions. It is proportional to $\boldsymbol{M}$: $\boldsymbol{\sigma} = \boldsymbol{\pi} + \beta(\boldsymbol{M} - m_0\boldsymbol{I})$, where β is the activity parameter and m_0 is a reference concentration for actomyosin. We use $m_0 = 1/2$ throughout. It can be explicitly derived for vertex models [44].

The dynamics of $\boldsymbol{M}(\mathbf{r}, t)$ is based on a myosin dissociation constant that decreases with tension. It follows from a contractile active junction that can remodel itself (see [44] and Supplemental Material Eqs. S1–S4 [46]). Since this is not sensitive to the precise functional form, we choose an exponential, controlled by susceptibility k_0 limiting the components of $\boldsymbol{M}$ to the range 0–1. In addition, the actomyosin tensor is convected and rotated by the flow,

$$\tau_m \mathring{\boldsymbol{M}} = \boldsymbol{I} - (\boldsymbol{I} + e^{-k_0\boldsymbol{\sigma}}) \cdot \boldsymbol{M} + D\nabla^2\boldsymbol{M}. \tag{1}$$

The over circle represents the corotational derivative $\mathring{\boldsymbol{A}} = \partial_t\boldsymbol{A} + \mathbf{v} \cdot \nabla\boldsymbol{A} + \boldsymbol{\omega} \cdot \boldsymbol{A} - \boldsymbol{A} \cdot \boldsymbol{\omega}$, where $\boldsymbol{\omega} = (1/2)[\nabla\mathbf{v} - (\nabla\mathbf{v})^T]$ is the vorticity tensor. We also include actomyosin diffusion with diffusion constant D.

The cell-cell junctions within the tissue are viscoelastic [47], as is the tissue as a whole, with a timescale of stress relaxation [48–51]. We use a convected compressible Maxwell model for the passive stress, superimposing compression and shear modes,

$$\boldsymbol{\pi} + \tau_v\mathring{\boldsymbol{\pi}} = \frac{1}{2}\eta_p \mathrm{Tr}(\dot{\boldsymbol{\gamma}})\boldsymbol{I} + \eta_s\left[\dot{\boldsymbol{\gamma}} - \frac{1}{2}\mathrm{Tr}(\dot{\boldsymbol{\gamma}})\boldsymbol{I}\right], \tag{2}$$

where τ_v is the viscous relaxation timescale, $\eta_p(\eta_s)$ are the bulk (shear) viscosities. The strain rate tensor is $\dot{\boldsymbol{\gamma}} = (1/2)[\nabla\mathbf{v} + (\nabla\mathbf{v})^T]$. The bulk and shear moduli are related to τ_v and the viscosities via $\tau_v = \eta_p/B = \eta_s/\mu$. The tissue is coupled to a substrate with friction coefficient ζ via momentum balance in the overdamped limit, $\zeta\mathbf{v} = \nabla \cdot \boldsymbol{\sigma}$.

Results.—We integrated the equations in time using the forward Euler method, approximating spatial derivatives using second order accurate finite difference on a square grid. The unit of time is the substrate elastic relaxation timescale $\tau_{el} = \zeta/B$, with both $\zeta = 1$ and bulk modulus $B = 1$, and we use a shear modulus $\mu = 0.5$. The myosin feedback strength is set by $k_0 = 8$ in Eq. (1) and β sets the active stress scale. We use a system size of $L = 50$ cell units with a grid spacing of 0.25 and we fix $D = 1$.

We simulate a patch inside a larger tissue by imposing a constant total stress $\boldsymbol{\sigma}_{\text{ext}}$ on the boundary while material flows through freely. Our model is neither incompressible nor density conserving as cells can reshape in the third dimension, and also can divide or be extruded [5]. We complement this with the equilibrium value $\boldsymbol{M} = (1 + e^{-k_0\boldsymbol{\sigma}^{\text{ext}}})^{-1}$ of the actomyosin tensor at the boundary and invert for the passive stress $\boldsymbol{\pi} = \boldsymbol{\sigma} - \beta(\boldsymbol{M} - m_0\boldsymbol{I})$. To study CE, we impose pure shear boundary conditions with simultaneous tension along x and compression along y as shown in Fig. 1, i.e., $\sigma^{\text{ext}}_{xx} = -\sigma^{\text{ext}}_{yy}$ and $\sigma^{\text{ext}}_{xy} = 0$, resulting in pure shear stress $\sigma_s \equiv \sigma^{\text{ext}}_{xx} - \sigma^{\text{ext}}_{yy}$, with the isotropic part of the applied stress $p \equiv \sigma^{\text{ext}}_{xx} + \sigma^{\text{ext}}_{yy} = 0$.

Figure 2 summarizes our findings. We measure tissue response using the spatially averaged pure shear strain rate $\dot{\gamma}_s \equiv \langle \dot{\gamma}_{xx} - \dot{\gamma}_{yy} \rangle$ of the steady state. We can see in Fig. 2(b) that at zero activity, $\dot{\gamma}_s = \sigma_s/\eta_s$, i.e., the tissue indeed behaves as a viscous liquid. Below a threshold activity $\beta_c = 0.5$, the tissue continues to flow in the direction of applied stress, and the effective viscosity stays positive. However, actomyosin is built up by active tension feedback and eventually overwhelms pulling when $\beta > \beta_c$. Figures 2(c) and 2(d) show how $\boldsymbol{M}_{xx}$ builds up in the tension direction, while $\boldsymbol{M}_{yy}$ symmetrically drops in the compression direction. Above β_c, the tissue then shows convergence extension [Fig. 2(a)] with the axis of elongation along the direction of compression, i.e., the tissue flows *against* the applied force. Actomyosin gradients and hence tissue flow is strongest near the boundary and decays into the bulk. The CE rheological curves above β_c in Fig. 2(b) are highly unusual: the tissue responds to $\sigma_s \to 0$ with a strongly symmetry broken CE, showing that the applied stress acts like a mechanical signal. When σ_s increases, the CE response diminishes, until at a β-dependent value the tissue flow reverses into the direction of pulling. For pure stretch or compression boundary conditions, i.e., $\sigma_s = 0$, $p \neq 0$, the tissue, respectively, isotropically contracts or expands above β_c (see Supplemental Material, Figs. S1–S4 for full spatial profiles [46]).

Analysis.—We can understand the observed spontaneous CE by approximating the nonlinear steady-state solutions of Eq. (1). From setting $\mathring{\boldsymbol{M}} = 0$, we can derive the actomyosin nullcline equations

$$\pi_{\alpha\alpha} = -\frac{1}{k_0}\log\left(M^{-1}_{\alpha\alpha} - 1\right) - \beta(M_{\alpha\alpha} - m_0), \tag{3}$$

where $\alpha = x, y$ and the off-diagonal components decay to zero [Fig. 3(b)]. The only fixed point of the viscoelastic passive stress is $\pi_{\alpha\alpha} = 0$, resulting in the transcendental equation $\pi_{\alpha\alpha}(M_{\alpha\alpha}) = 0$. Below $\beta_c = 0.5$, this equation has one stable solution, $M_{\alpha\alpha} = m_0$. Above the critical activity, there is a pitchfork bifurcation with two stable branches $M_{\alpha\alpha} = m^+ > m_0$ and $M_{\alpha\alpha} = m^- < m_0$, while the $M_{\alpha\alpha} = m_0$ branch becomes unstable [Fig. 3(a)].

During CE, the equal and opposite imposed boundary stresses select a pair of points (stars) on the nullcline that break symmetry, and at the center of the tissue, we find $M_{xx} = m^+$ and $M_{yy} = m^-$. The boundary conditions determine the branches: if we reverse tension and compression directions, we have $M_{xx} = m^-$ and $M_{yy} = m^+$ instead. Convergence extension flows are generated by the

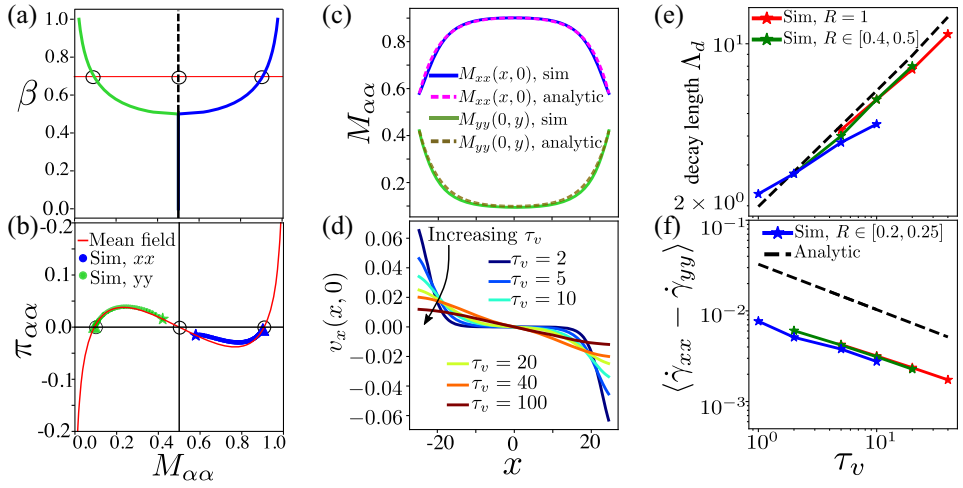

FIG. 3. (a) Pitchfork bifurcation of the mean field actomyosin concentration obtained via $\pi_{\alpha\alpha}(M_{\alpha\alpha}) = 0$ as a function of activity for $k_0 = 8$. (b) Mean field nullcline of $\dot{\boldsymbol{M}}$, $\pi_{\alpha\alpha}(M_{\alpha\alpha})$ (red) and corresponding simulation data for $\beta = 0.7$, $\sigma_s = 0.08$, $p = 0$, $\tau_m = \tau_v = 20.0$, with blue dots for $\pi_{xx}(M_{xx})$ along $y = 0$, green dots for $\pi_{yy}(M_{yy})$ along $x = 0$. The central (boundary) points are marked with a triangle (stars), and the three $\pi_{\alpha\alpha}(M_{\alpha\alpha}) = 0$ solutions with circles. (c) xx and yy components of the simulated (solid) and mean-field (dashed) $\boldsymbol{M}$ tensor for the same parameters as Fig. 2(c). (d) Simulated v_x velocity profiles in the CE state as a function of viscous timescale and for ratio $R = \tau_v/\tau_m \in [0.4 - 0.5]$, showing decay length. (e) Decay length and (f) pure strain rate in the CE phase as a function of τ_v together with mean field prediction (dashed).

spatial gradients in stress between boundary and center via momentum balance. We empirically observe that the values of these stresses interpolate between boundary and center points *along* the $\pi_{\alpha\alpha}(M_{\alpha\alpha})$ nullcline [Fig. 3(b)].

We can derive an approximate solution for the CE steady state by linearly expanding around the stable $\pi_{\alpha\alpha}(m^{\pm}) = 0$ fixed points and write $\pi_{xx}(M_{xx}) = \pi'(m^{+})m_x$, $\pi_{yy}(M_{yy}) = \pi'(m^{-})m_y$ where $m_x = M_{xx} - m^{+}, m_y = M_{yy} - m^{-}$, and set the off diagonal components to zero. We thus eliminate the actomyosin equation and once we use momentum balance to write $\dot{\boldsymbol{\gamma}}$, Eq. (2) for the stress to linear order in m_x and m_y becomes

$$\begin{aligned}\pi'(m^{+})(m_x + \tau_v \partial_t m_x) &= A_{+}\partial_x^2 m_x + A_{-}\partial_y^2 m_y,\\ \pi'(m^{-})(m_y + \tau_v \partial_t m_y) &= B_{+}\partial_y^2 m_y + B_{-}\partial_x^2 m_x,\\ 0 &= \partial_x \partial_y (C_{+} m_x + C_{-} m_y),\end{aligned} \quad (4)$$

where constants $A_{\pm}, B_{\pm}, C_{\pm}$ are given by Supplemental Material, Eq. S12 [46]. If we work in the limit $t \gg \tau_v$, we can neglect the time derivative resulting in coupled PDEs in x and y for $m_x(x, y)$ and $m_y(x, y)$. The final solution takes the form of a hyperbolic cosine in x and in y,

$$m_x = C_x \cosh\left[\frac{x}{\Lambda_{+}}\right] + C_y \cosh\left[\frac{y}{\Lambda_{\pm}}\right], \quad (5)$$

with the full solution and derivation given in Supplemental Material, Eqs. S10–S15 [46] and where the prefactors of each term are set by the boundary conditions. The length scale $\Lambda_{+} \sim \sqrt{(\eta_s + \eta_p)/\zeta}$, and we can derive the precise decay length (Supplemental Material, Eq. S17 [46]) $\Lambda_d \sim \sqrt{\tau_v}$, independent of τ_m of the $\boldsymbol{M}_{\alpha\alpha}$ profiles. Figure 3(c) shows that the analytic approximation closely matches the numerical solution, and Fig. 3(e) shows that both the value of Λ_d and the fact that it is τ_m independent are good predictions. The same ratio of viscosity to substrate friction then determines the penetration length of the gradient and therefore the extent of CE flow, as can be seen in the numerical velocity profiles in Fig. 3(d). We can derive an analytical prediction for the CE strain rate $\dot{\gamma}_s$, Supplemental Material Eq. S15 [46], shown as a dashed line together with the numerics in Fig. 3F, showing the same scaling.

Broader context.—In phase diagram Figs. 4(a) and 4(b), we show that other solutions than CE defined as steady-state time-independent flow opposite to applied stress, emerge in our model at large τ_v or τ_m. For very small τ_v if τ_m is large, the solution as expected localizes near the boundaries but $\boldsymbol{M}$ drops to the m_{-} solution throughout and we reach the time-independent expanding Loc Exp steady state as (Fig. S7 [46]). If we instead take the limit $\tau_v \to \infty$ at small τ_m, we observe pattern formation and regular oscillations in steady-state in the system, including for the first time a significant $\boldsymbol{M}_{xy}$ component [Figs. 4(c) and 4(d); Supplemental Material, Fig. S5 and movie "oscillating" [46]]. This is the Osc state, corresponding to the active *elastic* limit where our system behaves as an elastic solid with moduli B and μ coupled to the substrate with friction ζ. It has recently been shown that active instabilities and off-diagonal responses are a characteristic feature of active elastic systems with feedback [52–54] and that they also formally arise in viscoelastic systems [55]. Here, we show that they arise in a model for a biological tissue, raising the intriguing possibility that pattern formation in development could make use of such mechanisms.

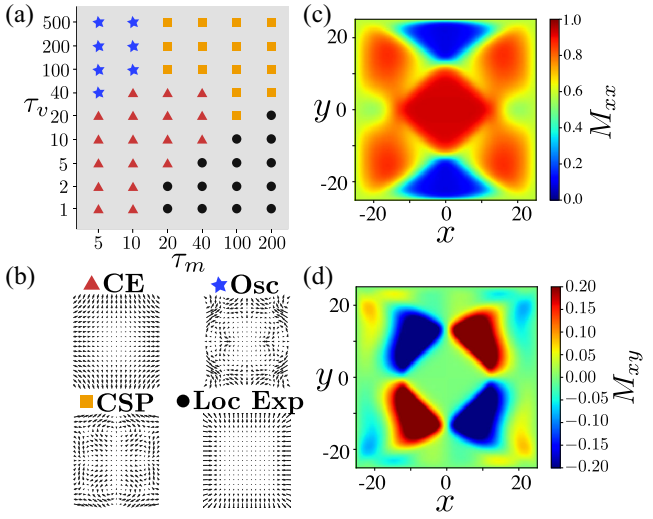

FIG. 4. Phases observed for other timescale ratios for $\beta = 0.7$, $\sigma_s = 0.08$, $p = 0$. (a) Observed phases as a function of viscous relaxation timescale τ_v and myosin timescale τ_m, in units of elastic substrate relaxation timescale $\tau_{\mathrm{el}} = \zeta/B = 1$. (b) Characteristic velocity fields of convergent-extension (CE), instability, oscillating, and localized expanding states. (c),(d) actomyosin wave pattern excited in the oscillating state for the M_{xx} (top) and off-diagonal M_{xy} (bottom) components.

In the limit of where $\tau_m, \tau_v \gg \tau_{el}$ (corresponding to the "wet" limit where substrate friction can be neglected), we observe a spatial destabilization of the CE pattern with complex spatiotemporal yet slow dynamics, which we refer to as the CSP (complex spatiotemporal pattern) phase (Supplemental Material, Fig. S6 and movie "CSP" [46]).

Our equations bear some similarities to active nematic systems, but only for the CE states which involve the traceless parts of $\boldsymbol{M}$ and $\boldsymbol{\pi}$. In contrast, isotropic contracting and expanding states are controlled by $\mathrm{Tr}(\boldsymbol{M})$ and $\mathrm{Tr}(\boldsymbol{\pi})$ (see Supplemental Material Eq. S20 [46]). We also do not find the generic instabilities usually observed. We observe instead robust and steady CE flows which is clearly very useful for biological functionality and control. While the friction with the substrate and the viscoelasticity act as stabilizers on short times and length scales, the key feature that keeps robust control is the interplay between the nonzero stress boundary conditions and the mechanochemical feedback of the actomyosin dynamics.

To explore this nice feature of the model and to compare to active nematics, we consider the dynamics of the traceless part of the actomyosin tensor, $\boldsymbol{Q}$, i.e., $\boldsymbol{M} = \boldsymbol{Q} + \frac{1}{2}\mathrm{Tr}(\boldsymbol{M})\boldsymbol{I}$. By expanding the matrix exponential in Eq. (1) to linear order in $\boldsymbol{Q}$, one can show that (see Supplemental Material, Eqs. S16–S27 [46])

$$\mathring{\boldsymbol{Q}} = a\boldsymbol{Q} + b\tilde{\boldsymbol{\pi}} + c\widetilde{\boldsymbol{\pi}\cdot\boldsymbol{Q}} + d\widetilde{\boldsymbol{Q}\cdot\boldsymbol{\pi}} + D\nabla^2\boldsymbol{Q} + \mathcal{O}(\boldsymbol{Q}^2), \quad (6)$$

where $\tilde{\boldsymbol{\pi}}$ is the traceless part of $\boldsymbol{\pi}$, $\widetilde{\boldsymbol{\pi}\cdot\boldsymbol{Q}}$ is the traceless part of $\boldsymbol{\pi}\cdot\boldsymbol{Q}$, $\widetilde{\boldsymbol{Q}\cdot\boldsymbol{\pi}}$ is the traceless part of $\boldsymbol{Q}\cdot\boldsymbol{\pi}$, $a = (1/2)\beta k_0 - 2$, $b = k_0/2$, $c = k_0(1 - \beta k_0/4)$, and $d = \beta k_0^2/4$. The first term shows that there is an isotropic to nematic transition at $\beta = 1/2$, the critical activity derived from our theory. For $\beta < 1/2$, we have a stable isotropic material. For $\beta > 1/2$, we have a nematic, however, the second term coming from the passive stress feedback at leading order resembles an applied field that will depend on boundary conditions. This field will in general suppress instabilities. The higher order terms will decorate this base state and can lead to a variety of interesting dynamical states, consistent with the simulations. While isotropic to nematic transitions driven by active flow have been observed in a variety of systems [56–58], here we provide a new mechanism for driving a transition to the nematic phase caused by mechanochemical feedback which resembles the application of an external field.

In summary, here we have introduced a continuum model of developmental tissues where convergence-extension flows arise wholly from mechanical feedback. We find robust CE flows where applied tension acts like an external field to determine the flow direction, based on breaking the symmetry of spontaneous actomyosin polarization. CE then arises from the active stress profile due to incommensurability between a bulk fixed point and the boundary conditions. Our model also shows pattern formation and spontaneous oscillations in the active elastic limit.

The authors would like to thank the Isaac Newton Institute for Mathematical Sciences, Cambridge, for support and hospitality during the programme "New statistical physics in living matter: non equilibrium states under adaptive control" where some of the work on this paper was undertaken. This was supported by EPSRC Grant No. EP/R014604/1. T. B. L. acknowledges the support of EPSRC Grant No. EP/T031247/1. T. B. L. acknowledges support of BrisSynBio, a BBSRC/EPSRC Advanced Synthetic Biology Research Centre (Grant No. BB/L01386X/1). S. H. acknowledges support of BBSRC Grant No. BB/N009150/2 and the University of Leiden. A. I. U. is funded by an EPSRC DTP studentship. The authors would like to thank Isaac Chenchiah, Ilyas Djafer Chérif, Rastko Sknepnek, Jake Turley, and Cornelis J. Weijer for in-depth discussions.

[1] R. J. Huebner and J. B. Wallingford, Dev. Cell **46**, 389 (2018).
[2] R. Keller, L. Davidson, A. Edlund, T. Elul, M. Ezin, D. Shook, and P. Skoglund, Phil. Trans. R. Soc. B **355**, 897 (2000).
[3] C. Bertet, L. Sulak, and T. Lecuit, Nature (London) **429**, 667 (2004).
[4] A. Sutherland, R. Keller, and A. Lesko, in *Seminars in Cell & Developmental Biology* (Elsevier, New York, 2020), Vol. 100, pp. 199–211.
[5] E. Rozbicki, M. Chuai, A. I. Karjalainen, F. Song, H. M. Sang, R. Martin, H.-J. Knölker, M. P. MacDonald, and C. J. Weijer, Nat. Cell Biol. **17**, 397 (2015).
[6] M. Saadaoui, D. Rocancourt, J. Roussel, F. Corson, and J. Gros, Science **367**, 453 (2020).
[7] M. Rauzi, P. Verant, T. Lecuit, and P.-F. Lenne, Nat. Cell Biol. **10**, 1401 (2008).
[8] M. Rauzi, U. Krzic, T. E. Saunders, M. Krajnc, P. Ziherl, L. Hufnagel, and M. Leptin, Nat. Commun. **6**, 8677 (2015).
[9] S. Höhn, A. R. Honerkamp-Smith, P. A. Haas, P. K. Trong, and R. E. Goldstein, Phys. Rev. Lett. **114**, 178101 (2015).
[10] A. Shindo, Wiley Interdiscip. Rev.: Syst. Biol. Med. **7**, e293 (2018).
[11] M. Durand and H. A. Stone, Phys. Rev. Lett. **97**, 226101 (2006).
[12] F. Graner, B. Dollet, C. Raufaste, and P. Marmottant, Eur. Phys. J. E **25**, 349 (2008).
[13] D. Weaire, Curr. Opin. Colloid Interface Sci. **13**, 171 (2008).
[14] C. Collinet, M. Rauzi, P.-F. Lenne, and T. Lecuit, Nat. Cell Biol. **17**, 1247 (2015).
[15] G. Odell, G. Oster, B. Burnside, and P. Alberch, J. Math. Biol. **9**, 291 (1980).
[16] H. Lan, Q. Wang, R. Fernandez-Gonzalez, and J. J. Feng, Phys. Biol. **12**, 056011 (2015).
[17] F. Bosveld, I. Bonnet, B. Guirao, S. Tlili, Z. Wang, A. Petitalot, R. Marchand, P.-L. Bardet, P. Marcq, F. Graner *et al.*, Science **336**, 724 (2012).
[18] G. H. Koenderink and E. K. Paluch, Curr. Opin. Cell Biol. **50**, 79 (2018).
[19] M. F. Lefebvre, N. H. Claussen, N. P. Mitchell, H. J. Gustafson, and S. J. Streichan, eLife **12**, e78787 (2023).
[20] H. J. Gustafson, N. Claussen, S. De Renzis, and S. J. Streichan, Nat. Commun. **13**, 7050 (2022).
[21] K. Dierkes, A. Sumi, J. Solon, and G. Salbreux, Phys. Rev. Lett. **113**, 148102 (2014).
[22] M. F. Staddon, K. E. Cavanaugh, E. M. Munro, M. L. Gardel, and S. Banerjee, Biophys. J. **117**, 1739 (2019).
[23] K. E. Cavanaugh, M. F. Staddon, S. Banerjee, and M. L. Gardel, Curr. Opin. Genet. Dev. **63**, 86 (2020).
[24] S. Banerjee, K. J. C. Utuje, and M. C. Marchetti, Phys. Rev. Lett. **114**, 228101 (2015).
[25] F. Pérez-Verdugo and S. Banerjee, arXiv:2211.05591.
[26] R. Etournay, M. Popović, M. Merkel, A. Nandi, C. Blasse, B. Aigouy, H. Brandl, G. Myers, G. Salbreux, F. Jülicher *et al.*, eLife **4**, e07090 (2015).
[27] N. Noll, M. Mani, I. Heemskerk, S. J. Streichan, and B. I. Shraiman, Nat. Phys. **13**, 1221 (2017).

[28] S. Tlili, E. Gauquelin, B. Li, O. Cardoso, B. Ladoux, H. Delanoë-Ayari, and F. Graner, R. Soc. Open Sci. **5**, 172421 (2018).
[29] K. Kruse, J.-F. Joanny, F. Jülicher, J. Prost, and K. Sekimoto, Eur. Phys. J. E **16**, 5 (2005).
[30] M. Popović, A. Nandi, M. Merkel, R. Etournay, S. Eaton, F. Jülicher, and G. Salbreux, New J. Phys. **19**, 033006 (2017).
[31] L. Giomi, M. J. Bowick, X. Ma, and M. C. Marchetti, Phys. Rev. Lett. **110**, 228101 (2013).
[32] G. Duclos, C. Blanch-Mercader, V. Yashunsky, G. Salbreux, J.-F. Joanny, J. Prost, and P. Silberzan, Nat. Phys. **14**, 728 (2018).
[33] G. Duclos, C. Erlenkämper, J.-F. Joanny, and P. Silberzan, Nat. Phys. **13**, 58 (2017).
[34] J.-M. Armengol-Collado, L. N. Carenza, J. Eckert, D. Krommydas, and L. Giomi, arXiv:2202.00668.
[35] T. B. Saw, A. Doostmohammadi, V. Nier, L. Kocgozlu, S. Thampi, Y. Toyama, P. Marcq, C. T. Lim, J. M. Yeomans, and B. Ladoux, Nature (London) **544**, 212 (2017).
[36] S. J. Streichan, M. F. Lefebvre, N. Noll, E. F. Wieschaus, and B. I. Shraiman, eLife **7**, e27454 (2018).
[37] M. Serra, S. Streichan, M. Chuai, C. J. Weijer, and L. Mahadevan, Proc. Natl. Acad. Sci. U.S.A. **112**, 11444 (2020).
[38] M. Chuai, G. Serrano Nájera, M. Serra, L. Mahadevan, and C. J. Weijer, Sci. Adv. **9**, eabn5429 (2023).
[39] M. Ibrahimi and M. Merkel, New J. Phys. **25**, 013022 (2023).
[40] D. Boocock, N. Hino, N. Ruzickova, T. Hirashima, and E. Hannezo, Nat. Phys. **17**, 267 (2021).
[41] D. Boocock, T. Hirashima, and E. Hannezo, PRX Life **1**, 013001 (2023).
[42] E. V. Sokurenko, V. Vogel, and W. E. Thomas, Cell Host Microbe **4**, 314 (2008).
[43] C. Veigel, J. E. Molloy, S. Schmitz, and J. Kendrick-Jones, Nat. Cell Biol. **5**, 980 (2003).
[44] R. Sknepnek, I. Djafer-Cherif, M. Chuai, C. Weijer, and S. Henkes, eLife **12**, e79862 (2023).
[45] M. Olenik, J. Turley, S. Cross, H. Weavers, P. Martin, I. V. Chenchiah, and T. B. Liverpool, Phys. Rev. E **107**, 014403 (2023).
[46] See Supplemental Material at http://link.aps.org/supplemental/10.1103/PhysRevLett.131.238301 for additional simulation results, a detailed derivation of the actomyosin equation, and the derivation of the traceless dynamics of M.
[47] R. Clément, B. Dehapiot, C. Collinet, T. Lecuit, and P.-F. Lenne, Curr. Biol. **27**, 3132 (2017).
[48] N. Khalilgharibi, J. Fouchard, N. Asadipour, R. Barrientos, M. Duda, A. Bonfanti, A. Yonis, A. Harris, P. Mosaffa, Y. Fujita *et al.*, Nat. Phys. **15**, 839 (2019).
[49] J. Ranft, M. Basan, J. Elgeti, J.-F. Joanny, J. Prost, and F. Jülicher, Proc. Natl. Acad. Sci. U.S.A. **107**, 20863 (2010).
[50] I. Bonnet, P. Marcq, F. Bosveld, L. Fetler, Y. Bellaïche, and F. Graner, J. R. Soc. Interface **9**, 2614 (2012).
[51] S. Tlili, M. Durande, C. Gay, B. Ladoux, F. Graner, and H. Delanoë-Ayari, Phys. Rev. Lett. **125**, 088102 (2020).
[52] C. Scheibner, A. Souslov, D. Banerjee, P. Surówka, W. T. Irvine, and V. Vitelli, Nat. Phys. **16**, 475 (2020).
[53] M. Brandenbourger, C. Scheibner, J. Veenstra, V. Vitelli, and C. Coulais, arXiv:2108.08837.
[54] T. H. Tan, A. Mietke, J. Li, Y. Chen, H. Higinbotham, P. J. Foster, S. Gokhale, J. Dunkel, and N. Fakhri, Nature (London) **607**, 287 (2022).
[55] D. Banerjee, V. Vitelli, F. Jülicher, and P. Surówka, Phys. Rev. Lett. **126**, 138001 (2021).
[56] S. Santhosh, M. R. Nejad, A. Doostmohammadi, J. M. Yeomans, and S. P. Thampi, J. Stat. Phys. **180**, 699 (2020).
[57] R. Mueller, J. M. Yeomans, and A. Doostmohammadi, Phys. Rev. Lett. **122**, 048004 (2019).
[58] T. Markovich, E. Tjhung, and M. E. Cates, Phys. Rev. Lett. **122**, 088004 (2019).